Isolation and suppression of forced oscillations through wind farms under grid following and grid forming control

Zhao, Xianxian; Xue, Ying; Zhang, Xiao-Ping

DOI:
10.1109/ACCESS.2021.3082166

Document Version
Publisher's PDF, also known as Version of record

Citation for published version (Harvard):
Zhao, X, Xue, Y & Zhang, X-P 2021, 'Isolation and suppression of forced oscillations through wind farms under grid following and grid forming control', *IEEE Access*, vol. 9, pp. 76446 - 76460. https://doi.org/10.1109/ACCESS.2021.3082166

IEEE Access
Multidisciplinary | Rapid Review | Open Access Journal

IEEE POWER & ENERGY SOCIETY SECTION

Received May 3, 2021, accepted May 17, 2021, date of publication May 20, 2021, date of current version June 1, 2021.

Digital Object Identifier 10.1109/ACCESS.2021.3082166

Isolation and Suppression of Forced Oscillations Through Wind Farms Under Grid Following and Grid Forming Control

XIANXIAN ZHAO[1,2], YING XUE[2], (Member, IEEE), AND XIAO-PING ZHANG[2], (Fellow, IEEE)

[1]School of Electrical and Electronic Engineering, University College Dublin, Dublin 4, D04 V1W8 Ireland
[2]Department of Electronic, Electrical and Systems Engineering, University of Birmingham, Birmingham B15 2TT, U.K.

Corresponding author: Xiao-Ping Zhang (x.p.zhang@bham.ac.uk)

This work was supported in part by the Engineering and Physical Sciences Research Council (EPSRC) under Grant EP/N032888/1 and Grant EP/L017725/1.

ABSTRACT Forced Oscillations can occur even for a power system with good damping performance. With increasing high penetration of renewable energy generation towards 100% renewable generation in the power grid, exploitation of future control potential from wind turbines becomes inevitable. This paper develops an isolation and suppression method of Forced Oscillations by using wind farms (WFs) under both grid-following and grid-forming control principles. The proposed method controls a WF to absorb or release active and reactive power in a timely manner and as a result Forced Oscillations are prevented from spreading to the rest of the power grid and hence they are isolated. The Forced Oscillations of the disturbed area, which is bounded by the location of WF installation, are also reduced and suppressed. The proposed method is easy to implement and economically effective as there is no requirement of extra energy storage and power electronic devices, and a prior knowledge of the frequency of Forced Oscillations is not required. With the proposed control method, the loss of wind power capture is negligible. Furthermore, the control method is also able to damp natural oscillations. Simulations of both doubly fed induction generator (DFIG)-, and permanent magnetic synchronous generator (PMSG)-based WFs under either grid-following or grid-forming control principle, with constant or varying wind speeds and different WF locations with respect to the source of Forced Oscillations, on the modified two-area and IEEE 39-bus power systems, using Real-time Digital Simulator (RTDS) and Dymola, are used to verify the effectiveness of the proposed method.

INDEX TERMS Energy storage, forced oscillations, grid-following, grid-forming, inter-area oscillations, wind farm, wind turbine, permanent magnetic synchronous generator (PMSG), doubly fed induction generator (DFIG).

I. INTRODUCTION

Compared to intrinsic natural interactions among dynamic components due to low or negative damping of a system [1], Forced Oscillations are incurred by periodic external disturbances at frequencies close or equal to the natural frequencies of the system modes and have been observed in power systems [2]–[9]. Those external periodic disturbances include cyclic loads, electrical oscillations caused by malfunctions of power system stabilizers (PSSs) in power plants, mechanical oscillations of synchronous generator turbines, and periodically fluctuating wind power due to wind shear and tower shadow effects [2]. Compared with natural oscillations, Forced Oscillations exhibit much higher magnitude and may cause catastrophic consequences, especially under the poorly damped operating conditions [4], [8], [9].

Considering the origins and characteristics, countermeasures for Forced Oscillations are different from those for natural oscillations. Generally, there are three categories of methods to minimize the adverse impact from Forced Oscillations, namely, (a) Elimination of Forced Oscillations; (b) Damping of Forced Oscillations; and (c) Isolation and suppression of Forced Oscillations. The first category of methods aims to completely eliminate Forced Oscillations by removing the external fluctuating forces [4], [10]; however, this removal is difficult and sometimes even impossible

The associate editor coordinating the review of this manuscript and approving it for publication was Guangya Yang.

to realize due to two reasons: (1) It requires accurate and timely locating of external fluctuating forces, which is difficult to achieve. Many online localization methods such as graph-theoretic method [11], forecasting-residual spectrum analysis method [12], energy-based method [13] and synchrophasor data based harmonic analysis method [14] have been proposed, but the methods proposed in [11], [12] rely on accurate system models, in [13] the relationship between the relative oscillation energy and the actual oscillating active power is unclear, and in [14] the scheme may be imprecise, for example when only a few buses in the network have synchrophasors; and (2) The external perturbation sources can be small or within some critical power plants or loads, making it neither practical nor economic to remove [3].

In the second category of methods, instead of a complete elimination of Forced Oscillations, increasing system damping in [15]–[17], shifting the resonant frequency using a unified power flow controller [18], and injecting oscillating active power of utility energy storage systems in [19] are proposed to suppress Forced Oscillations. However, unlike natural oscillations which can be attenuated quickly when the damping of the system is improved, Forced Oscillations can still occur, be sustained [8], [9], and spreading around the whole power system. Moreover, the methods in [16], [17] that relies on wide-area measurements and a central controller and the method in [18] that requires Forced Oscillations detection limit practical applications. Moreover, in [18] by shifting the resonant frequency Forced Oscillations can still sustained and spread the whole power system.

The third category of methods aims to isolate and suppress Forced Oscillations. Based on such methods, the propagation of Forced Oscillations from the disturbed generator/area to the rest of the power grid is stopped, and subsequently, the Forced Oscillations of the disturbed generator/area can be reduced. In [3] an E-STATCOM approach was proposed to isolate and suppress Forced Oscillations by incorporating an energy storage unit into static synchronous compensator (STATCOM). The disadvantages of this method are twofold: (1) Extra power electronic hardware and energy storage devices are required, and the cost and maintenance requirements of the associated devices must be considered; (2) Resonant controllers are adopted that require a priori knowledge of the frequency of the external disturbance. In [20] the installation of an extra flywheel was proposed to smooth the wind power of a wind farm (WF) due to wind shear and tower shadow effects which would induce Forced Oscillations in the power system. Instead of installing an extra flywheel, in [21] the DC-link capacitor was utilized in a permanent magnetic synchronous generator (PMSG)-based wind turbine systems (WTS) with the same power compensation control as that in [20] to smooth the wind power of a WF. However, the method proposed in [20] will need to install extra flywheel energy storage systems, and the one in [21] has limited suppression capability due to the small energy storage capacity of the DC-link capacitor. In [22], the controllable devices are tuned to inject a second oscillation into the grid to compensate the oscillations of a designated point in the system. Based on tuned feedback control, it requires accurate estimation of the system's frequency response and Forced Oscillation frequency. Moreover, the simulation results shows that the method provides only around 90% suppression.

With increasing high penetration of renewable energy generation towards 100% renewable generation in the power grid, exploitation of future control potential from wind turbines becomes inevitable. This paper proposes an isolation and suppression method targeting at Forced Oscillations by WFs through controlling the large kinetic energy of WFs below rated wind speed and utilizing external wind energy above rated wind speed. With the proposed method the WF can timely release or absorb active and reactive power opposite to the oscillating power from the disturbed area. As a result, the Forced Oscillations are prevented from propagating to the rest of the power grid and hence be isolated. The Forced Oscillations of the disturbed area that is bounded by the location of WF installation are also suppressed. This paper has the following key contributions:

- The proposed method is the first of its kind by using WFs to isolate and suppress Forced Oscillations. Thus, no extra energy storage and power electronic converters need to be installed. Simulation results demonstrated that both the loss of wind power and the increase of the capacity of converters are small.
- The proposed method can be easily implemented with only the information of the oscillating active and reactive power from the disturbed area, while a prior knowledge of frequencies of Forced Oscillations is not required.
- Although the primary objective of the proposed method is to suppress Forced Oscillations, it is also helpful to damp natural oscillations.
- The proposed isolation and suppression method of Forced Oscillations is designed and validated for WTSs under either grid-following or grid-forming control principles.

The paper is organized as follows. Section II illustrates the principle of the proposed method and analyzes the characteristics of Forced Oscillations in a power system without and with the proposed method. Section III illustrates the realization of the proposed method in a WTS under either grid-following or grid-forming control principles. Section IV verifies the performance of the proposed method by simulations on a modified two-area and 39-bus power systems. Finally, Section V provides the conclusions.

II. PRINCIPLES OF THE PROPOSED ISOLATION AND SUPPRESSION OF FORCED OSCILLATIONS

In this section, the principles of the proposed isolation and suppression method are first described. Then the characteristics of the Forced Oscillations excited by an external periodic disturbance in the disturbed area that is bounded by the location of WF installation without and with the proposed isolation and suppression by WF are analyzed.

A. PRINCIPLES OF THE PROPOSED METHOD

This section describes the principles of the proposed method. To help illustrate the method, a two-machine system with a WF is considered, as shown in Fig. 1, where synchronous generator 1 (SG1) and synchronous generator 2 (SG2) are used to represent two areas of a power system. An external disturbance ΔP_m is added to the mechanical power of SG1, causing Forced Oscillations in the system. P_{ij} and Q_{ij} are the transferred active and reactive power between bus i and bus j, $\overline{P_{ij}}$ and $\overline{Q_{ij}}$ are obtained by applying a low-pass filter or moving average filter to P_{ij} and Q_{ij} respectively. P_{mppt} is the maximum power output of WF under MPPT control, which is implemented by applying a low-pass filter or moving average filter and will be explained further in Section III, and ε represents the loss of wind power capture under the proposed control. As will be demonstrated by simulation results in Section IV, ε is very small, and thus can be neglected.

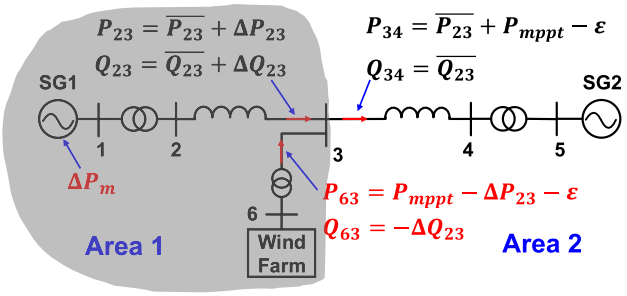

FIGURE 1. A two-machine system with a WF to illustrate the proposed method.

As illustrated in Fig. 1, the WF injects extra oscillating active and reactive power by controlling the WF to isolate Forced Oscillations, which are given by

$$\Delta P_{inj} = -\Delta P_{23} \tag{1}$$

$$\Delta Q_{inj} = -\Delta Q_{23} \tag{2}$$

Thus, P_{34} and Q_{34} are

$$P_{34} = P_{23} + P_{63} = \overline{P_{23}} + P_{mppt} - \varepsilon \tag{3}$$

$$Q_{34} = Q_{23} + Q_{63} = \overline{Q_{23}} \tag{4}$$

In this way, P_{34} and Q_{34} being injected into Area 2 do not contain oscillating components. Therefore, the transmission line T2-3 between bus 2 and bus 3 becomes the *isolation wall* through which the Forced Oscillations cannot propagate and are only contained within Area 1. When the Forced Oscillations in Area 1 are isolated and prevented from transmitting to Area 2, the oscillations in Area 1 are also suppressed, which will be analyzed in Section B.

Remark 1: As shown in (1) and (2) since the input signals are the measured power of the adjacent transmission lines connected at the Point of Common Coupling (PCC) of the WF, the proposed control does not need a prior knowledge of frequencies of the Forced Oscillations and is able to respond to any power fluctuations, not only the Forced Oscillations but also natural oscillations including inter-area oscillations. Moreover, the power measurement units only need to be installed at the adjacent transmission lines.

Remark 2: As stated in [3] and can be seen from Fig. 1, if the WF is closer to the disturbed source SG1, a bigger area will be immune from Forced Oscillations and the excited oscillating power output of SG1 will be smaller (which will be analyzed in Section B).

Remark 3: In [3] to make ΔP_{34} and ΔQ_{34} zero, resonance control is used with ΔP_{34} and ΔQ_{34} as input and the prior knowledge of the oscillating frequency of ΔP_{34} and ΔQ_{34} is required. As seen from (1)-(4) the proposed control can also make ΔP_{34} and ΔQ_{34} zero by using ΔP_{23} and ΔQ_{23} as inputs. Thus, in principle the two methods can have the same performance to isolate and suppress Forced Oscillations. But it should be pointed out that the performance of the proposed method will be limited when there is no wind or very low wind speed (although the probability of such situation is low as can be seen from the wind speed probability distributions in [23], [24]). However, the proposed method can still be used if energy storage equipment is installed in the WF when there is no wind or very low wind speed. Considering the higher penetration of renewable energy and progress in energy storage technology, WFs being equipped with energy storage will become more likely in the future.

Remark 4: The principle of choosing *isolation walls* is to enclose a region that has Forced Oscillation sources. The isolation walls will be selected to make sure the region is sufficiently small. If the enclosed region is re-connected to the rest of the grid due to grid topology changes, the *isolation walls* need to be re-chosen to enclose a new region that contains the Forced Oscillation sources, but the control of the proposed method does not need to change and can be equally applied.

Remark 5: The proposed isolation method does not need disconnection of Forced oscillation sources. The principle of the proposed method is injecting oscillating power to the grid to cancel the oscillating power of the selected transmission lines (i.e. *isolation walls*). In this way, the Forced oscillations will be isolated within a smaller area enclosed by the *isolation walls* and not spreading to the rest of the grid. Within this area, the amplitudes of the Forced oscillations will also be suppressed.

Remark 6: The proposed method can also isolate the Forced Oscillations that could be excited by the oscillating power of WFs. This is because the oscillating wind power is smoothed by using the average instead of real-time rotor speeds of WTSs in the proposed control, as can be seen in (27) and (31) in the next section.

Remark 7: In the proposed method, Forced Oscillations do not need to be estimated, since the input signal to the WF is the measured power at the adjacent transmission line(s) connected at the PCC of the WF, as can be seen in equations (1) and (2). In a large meshed power grid, such an estimation of the disturbances is still not required, but several WFs may be needed to enclose an isolated area that has Forced Oscillation sources (which will be demonstrated in Case 8 in section IV).

B. CHARACTERISTICS OF EXCITED FORCED OSCILLATIONS WITHOUT AND WITH THE PROPOSED ISOLATION AND SUPPRESSION METHOD USING WF

This section will illustrate the characteristics of excited Forced Oscillations without and with the proposed method described in Section A, to rationalize the design of the proposed method and to quantify the suppression effect on Forced Oscillations in the isolated area by the proposed method. The equivalent circuit of Fig. 1 is shown in Fig. 2, where the losses in the transmission system are neglected for simpler analysis, and the WF is modelled as a controlled current source supplying active power $P_{mppt} + \Delta P_{inj}$ and reactive power ΔQ_{inj} into the network. P_{fo} and Q_{fo} are the active and reactive power transferred to the PCC of the WF from SG1.

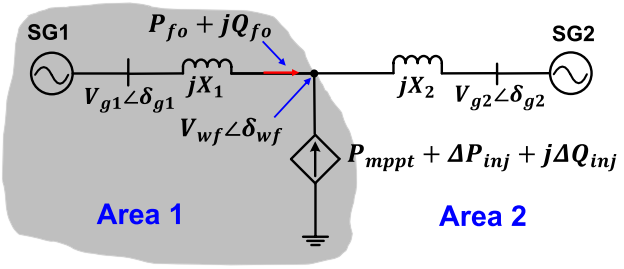

FIGURE 2. Equivalent circuit for the two-machine system with the WF modelled as a controlled current source.

1) FORCED OSCILLATIONS WITHOUT THE PROPOSED METHOD

This subsection theoretically analyzes the characteristics of Forced Oscillations without the proposed method and therefore rationalize the design of the proposed method. The external disturbance ΔP_m of SG1 causes oscillations of rotor speed and rotor angle of SG1, and further lead to active and reactive power oscillations in the system. When ΔP_{inj} and ΔQ_{inj} are zero (i.e., WF is not controlled to isolate and suppress Forced Oscillations), the active and reactive power transfers can be written as

$$P_{fo} = \frac{V_{g1}V_{wf}\sin(\delta_{g1} - \delta_{wf})}{X_1},$$

$$Q_{fo} = \frac{V_{g1}V_{wf}\cos(\delta_{g1} - \delta_{wf}) - V_{wf}^2}{X_1} \quad (5)$$

$$P_{fo}+P_{mppt} = \frac{V_{g2}V_{wf}\sin(\delta_{wf} - \delta_{g2})}{X_2} \quad (6)$$

Assuming SG2 as reference machine, i.e. $\delta_{g2} = 0$, linearizing the equations of motion of SG1 and (5) and (6), the following equations can be obtained

$$M_1\frac{d(\Delta\omega_{g1})}{dt} = \Delta P_m - \Delta P_{fo} - D_1\Delta\omega_{g1} \quad (7)$$

$$\frac{d(\Delta\delta_{g1})}{dt} = \omega_b\Delta\omega_{g1} \quad (8)$$

$$\Delta P_{fo} = K_{P\delta}\Delta\delta_{g1} \quad (9)$$

$$\Delta Q_{fo} = K_{Q\delta}\Delta\delta_{g1} \quad (10)$$

where

$$K_{P\delta} = \frac{V_{g10}V_{wf0}\cos(\delta_{g10} - \delta_{wf0})}{X_1} \times [1 - \frac{X_2V_{g10}\cos(\delta_{g10} - \delta_{wf0})}{X_1V_{g20}\cos\delta_{wf0} + X_2V_{g10}\cos(\delta_{g10} - \delta_{wf0})}] \quad (11)$$

$$K_{Q\delta} = -\frac{V_{g10}V_{wf0}\sin(\delta_{g10} - \delta_{wf0})}{X_1} \times [1 - \frac{X_2V_{g10}\cos(\delta_{g10} - \delta_{wf0})}{X_1V_{g20}\cos\delta_{wf0} + X_2V_{g10}\cos(\delta_{g10} - \delta_{wf0})}] \quad (12)$$

In (7)-(8), M_1 and D_1 are inertia constant and damping factor of SG1 respectively, ω_b is the base angle electrical speed in radians per second, and in (11)-(12) the subscript 0 represents the corresponding variables at steady-state.

Combining (7)-(10), the transfer function $G_{Pfo}(s)$ and $G_{Qfo}(s)$ from ΔP_m to ΔP_{fo} and ΔQ_{fo}, respectively, can be obtained as

$$G_{Pfo}(s) = \frac{\omega_bK_{P\delta}}{M_1s^2 + D_1s + \omega_bK_{P\delta}} = \frac{\omega_n^2}{s^2 + 2\zeta\omega_ns + \omega_n^2} \quad (13)$$

$$G_{Qfo}(s) = \frac{K_{Q\delta}}{K_{P\delta}}G_{Pfo}(s) \quad (14)$$

where ω_n and ζ are the undamped natural frequency and damping ratio of $G_{Pfo}(s)$ and $G_{Qfo}(s)$, given by

$$\omega_n = \sqrt{\frac{\omega_bK_{P\delta}}{M_1}} \quad (15)$$

$$\zeta = \frac{1}{2}\frac{D_1}{\sqrt{\omega_bM_1K_{P\delta}}} \quad (16)$$

The bode plots of $G_{Pfo}(s)$ and $G_{Qfo}(s)$ are shown in Fig. 3 where the damping factor D_1 is deliberately set as 10 per-unit (pu). It can be seen that around the undamped natural frequency ω_n, the magnitudes of both transfer functions become much larger, which means that large-magnitude oscillations (Forced Oscillations) happen even when the damping is large. Also, it can be seen that the magnitude of $G_{Pfo}(s)$ is much larger than that of $G_{Qfo}(s)$, which means that Forced Oscillations are mainly associated with active power in an inductive system.

The largest magnitude of $G_{Pfo}(s)$ at ω_n is given by

$$|G_{Pfo}(j\omega_n)| = \frac{1}{2\zeta} = \frac{\sqrt{\omega_bM_1K_{P\delta}}}{D_1} \quad (17)$$

Equation (17) shows:

- The magnitude of the excited Forced Oscillations can be reduced by increasing damping D_1, or decreasing inertia constant M_1.
- The Forced Oscillations cannot be eliminated unless D_1 is infinite (which is impossible), or the external disturbance ΔP_m is removed (which is difficult or impossible to achieve). Therefore, this paper proposes to use WF to inject extra power (especially active power) to isolate and suppress the Forced Oscillations.

2) FORCED OSCILLATIONS IN THE DISTURBED AREA WITH THE PROPOSED METHOD

This subsection theoretically analyzes the suppression effect on Forced Oscillations in the isolated area by the proposed method. Based on [25], the change of amplitude and angle of $V_{wf}\angle\delta_{wf}$ due to injection of ΔP_{inj} and ΔQ_{inj} are

$$\Delta V_{wf} \approx \frac{X_1X_2}{(X_1+X_2)V_{wf0}}\Delta Q_{inj},\ \ \Delta\delta_{wf} \approx \frac{X_1X_2}{(X_1+X_2)V_{wf0}^2}\Delta P_{inj} \tag{18}$$

Using superposition principle, the new $\Delta P'_{fo}$ and $\Delta Q'_{fo}$ under the impact of ΔP_m and ΔP_{inj} and ΔQ_{inj} are given by,

$$\Delta P'_{fo} = K_{P\delta}\Delta\delta_{g1} - K_{PP}\Delta P_{inj} - K_{PQ}\Delta Q_{inj} \tag{19}$$

$$\Delta Q'_{fo} = K_{Q\delta}\Delta\delta_{g1} - K_{QP}\Delta P_{inj} - K_{QQ}\Delta Q_{inj} \tag{20}$$

where K_{PP}, K_{PQ}, K_{QP} and K_{QQ} are

$$K_{PP} = \frac{(1-a)V_{g10}\cos(\delta_{g10}-\delta_{wf0})}{V_{wf0}} \tag{21}$$

$$K_{PQ} = -\frac{(1-a)V_{g10}\sin(\delta_{g10}-\delta_{wf0})}{V_{wf0}} \tag{22}$$

$$K_{QP} = -\frac{(1-a)V_{g10}\sin(\delta_{g10}-\delta_{wf0})}{V_{wf0}} \tag{23}$$

$$K_{QQ} = 2(1-a) - \frac{(1-a)V_{g10}\cos(\delta_{g10}-\delta_{wf0})}{V_{wf0}} \tag{24}$$

where $a = X_1/(X_1+X_2)$, representing the electrical distance of the WF to SG1.

The coefficients shown in (21) $\sim$ (24) with changing a (i.e., changing electrical distance of the WF to SG1) are shown in Fig. 4 under two operating conditions of $P_{g10} = 0.9\ pu$ and $P_{g10} = 0.1\ pu$. It can be seen from Fig. 4 that both K_{PQ}, K_{QP} are very small under two operation conditions. Ignoring K_{PQ} and K_{QP} combining (7)-(8) and (19)-(20), the transfer function from ΔP_m to $\Delta P'_{fo}$ and $\Delta Q'_{fo}$ are given by

$$G'_{Pfo}(s) = \frac{\omega_b K_{P\delta}}{(1-K_{PP})(M_1s^2+D_1s)+\omega_b K_{P\delta}} = \frac{\omega_n^2}{(1-K_{PP})(s^2+2\zeta\omega_n s)+\omega_n^2} \tag{25}$$

$$G'_{Qfo}(s) = \frac{(1-K_{PP})K_{Q\delta}}{(1-K_{QQ})K_{P\delta}}G'_{Pfo}(s) \tag{26}$$

The bode plots of $G'_{Pfo}(s)$ and $G'_{Qfo}(s)$ are also shown in Fig. 3. Comparing $G'_{Pfo}(s)$ and $G'_{Qfo}(s)$ in (25) and (26) (with the proposed method) with $G_{Pfo}(s)$ and $G_{Qfo}(s)$ in (13) and (14) (without the proposed method), it can be seen from Fig. 3 that the magnitude of the excited active power oscillation at ω_n is decreased from point A to point B, and the magnitude of the excited reactive power oscillation at ω_n is decreased from point C to point D, meaning the forced oscillations in disturbed area are suppressed.

Fig. 5 shows $|G'_{Pfo}(j\omega_n)|$ and $|G_{Pfo}(j\omega_n)|$ with relation to the electrical distance a of the WF to SG1 under two operating conditions. It can be seen that with smaller a, the suppression effect of Forced Oscillations in disturbed area is better. Therefore, in practice, it is better to choose WFs to enclose Forced Oscillations to be within a smaller area. In this way, a larger area is immune from Forced Oscillations. Moreover, the Forced Oscillations excited in the disturbed area can be better suppressed.

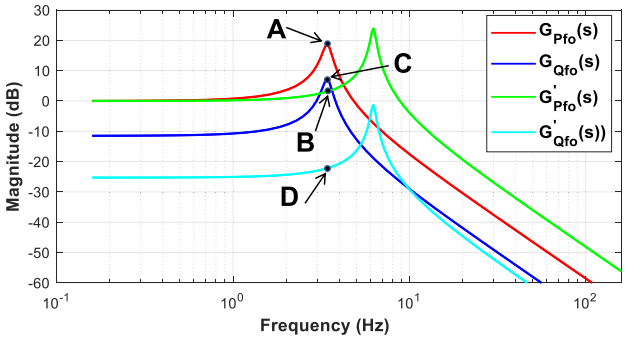

FIGURE 3. Bode diagrams of $G_{Pfo}(s)$ and $G_{Qfo}(s)$, $G'_{Pfo}(s)$ and $G'_{Qfo}(s)$ from external disturbance ΔP_{m1} to ΔP_{g1} and ΔQ_{g1} of SG1 of the system in Fig. 1 where $M_1 = 4\ pu$, $D_1 = 10\ pu$, $\omega_b = 377\ rad/s$, $X_1 = 0.06\ pu$, $X_2 = 0.14\ pu$, $V_{g10} = V_{wf0} = V_{g20} = 1\ pu$ and $P_{wf0} = 0.6\ pu$.

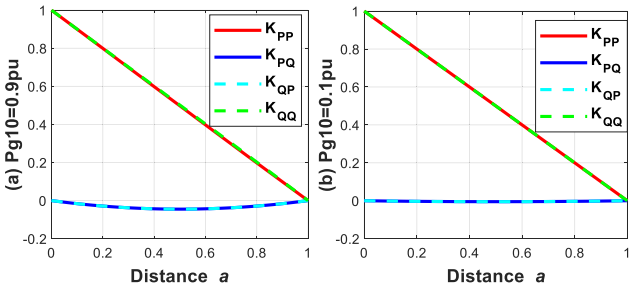

FIGURE 4. The relationship of K_{PP}, K_{PQ}, K_{QP} and K_{QQ} with the electrical distance of the WF to SG1 a under two operation conditions, where $M_1 = 4\ pu$, $D_1 = 10\ pu$, $\omega_b = 377\ rad/s$, $X_1 + X_2 = 0.2\ pu$, $V_{g10} = V_{wf0} = V_{g20} = 1\ pu$. (a) $P_{g10} = 0.9\ pu$. (b) $P_{g10} = 0.1\ pu$.

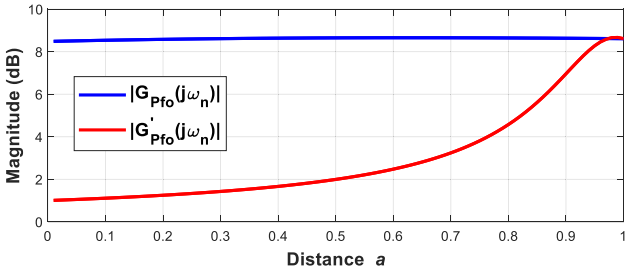

FIGURE 5. $|G'_{Pfo}(j\omega_n)|$ and $|G_{Pfo}(j\omega_n)|$ vs. the distance of WF to SG1 a under two operation conditions of $P_{g10} = 0.9\ pu$ where the parameters are the same as that in Fig. 4.

III. REALIZATION OF THE PROPOSED METHOD IN A WTS UNDER GRID-FOLLOWING AND GRID-FORMING CONTROL

In this section, the realization of the proposed isolation and suppression of Forced Oscillations method in a WTS under grid-following and grid-forming control is described.

A. THE PROPOSE METHOD REALIZED IN A GRID-FOLLOWING WTS

Fig. 6 shows the configuration and control structure of the proposed Forced Oscillation isolation and suppression method in a PMSG-based WTS under grid-following control as an example [26]. The grid side converter GSC uses a phase-locked-loop (PLL) to track the grid voltage frequency and angle, so that the generated voltage of the GSC is synchronized to the grid voltage. Thus, the WTS is controlled based on ''grid-following'' control principle. Under such control, a WTS does not actively regulates system voltage frequency and amplitude. It thus weakens the system, and leads to a weaker grid when there is a higher share of grid-following WTSs.

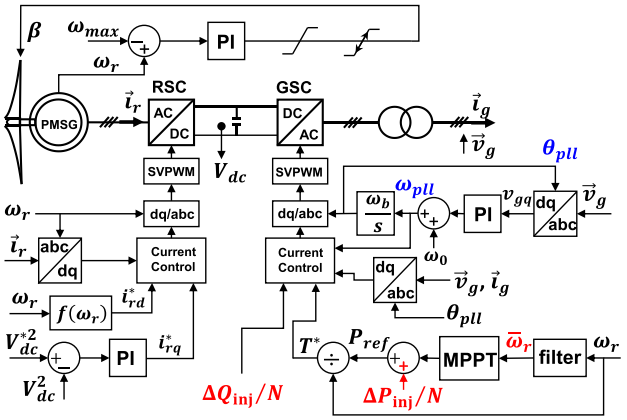

FIGURE 6. Control structure of the proposed Forced Oscillation isolation and suppression in a PMSG-based WTS under grid-following control, where $\vec{i_r}$, $\vec{i_g}$, $\vec{v_g}$: current and voltage at rotor side and grid side, V_{dc}: DC-link voltage, β: pitch angle, ω_r: rotor speed, ω_{pll}, θ_{pll}: the tracked grid voltage frequency and angle by the phase-locked-loop (PLL), ΔP_{inj}, ΔQ_{inj}: given by (1) and (2).

In Fig. 6, the wind turbine captures power from wind [27]. The pitch-angle controller is used to limit the rotor speed under high wind speed. It becomes effective when $\omega_r > \omega_{\max}$ ($\omega_{\max} = 1$ pu in this paper). The rotor-side converter (RSC) is to stabilize the DC-link voltage and performs approximately zero reactive power output from the PMSG to minimize losses, while the grid-side converter (GSC) has four functions:

1) Performing the maximum wind power capture;

2) Smoothing oscillating wind power caused by variable wind speed which would excite Forced Oscillations;

3) Injecting ΔP_{inj} by controlling the large kinetic energy of WTSs below the rated wind speed and utilizing the external wind energy above the rated wind speed to isolate the active power part of Forced Oscillations;

4) Injecting ΔQ_{inj} by using capability of the converter to isolate the reactive power part of Forced Oscillations. The reactive power control is independent from the active power control.

In order to realize the above four functions, the active and reactive power references of the GSC are given by

$$P_{ref} = K_{opt}\overline{\omega}_r^3 + \frac{\Delta P_{inj}}{N} \tag{27}$$

$$Q_{ref} = \frac{\Delta Q_{inj}}{N} \tag{28}$$

where K_{opt} is the optimal coefficient, N is the total number of WTSs in a WF, ΔP_{inj} and ΔQ_{inj} are given by (1) and (2), and $\overline{\omega_r}$ is the average of ω_r through a low-pass filter or moving average filter.

Comparing with classic MPPT control where the active and reactive power references are given by $P_{mppt} = K_{opt}\omega_r^3$ and $Q_{ref}^{mppt} = 0$, the control design in (27)(28) can realize the above first four functions, because:

1) $K_{opt}\overline{\omega}_r^3$ gives a smoother power reference than $K_{opt}\omega_r^3$ so that oscillating wind power output that could excite Forced Oscillations can be smoothed;

2) The components $\Delta P_{inj}/N$ and $\Delta Q_{inj}/N$ in (27) and (28) respectively can make the WTS generate oscillating power opposite to Forced Oscillations on the adjacent transmission lines. Thus, these transmission lines become *isolation walls* through which the Forced Oscillations cannot propagate into other areas.

3) Since the rotor speed under the proposed control is only slightly deviated from that under the MPPT control, the maximum wind power capture can also be realized, which will be demonstrated in Section IV.

It should be noted that under a high wind speed when the pitch angle control is effective and ω_r is constant, the Forced Oscillations isolation and suppression method is also effective. In this case, the utilized energy comes from the external wind instead of the stored kinetic energy in a WTS.

B. THE PROPOSE METHOD REALIZED IN A GRID-FORMING WTS

With reference to Fig. 7, there is an example configuration and control structure of a PMSG-based WTS under grid-forming control principle for implementing the discussed Forced Oscillation isolation and suppression method. The discussed method could also be implemented using other types of wind turbine system such as a doubly fed induction generator (DFIG)-based WTS [28], other power electronics-interfaced variable speed wind turbine system with induction generator, and synchronous generator (not shown), under either grid-following or grid-forming control principle.

The control of the rotor-side converter RSC and pitch-angle controller of the system in Fig. 7 are the same as that in Fig. 6. But the grid-side converter GSC in Fig. 7 is now controlled as a grid-forming converter. Different from the GSC in Fig. 6 of using a PLL to follow the grid voltage frequency and phase, the GSC in Fig. 7 generates the frequency ω_{vsm} and phase θ_{vsm} and amplitude V_o^* for its output voltage $\vec{v_o}$. Therefore, it spontaneously regulates the grid voltage frequency and

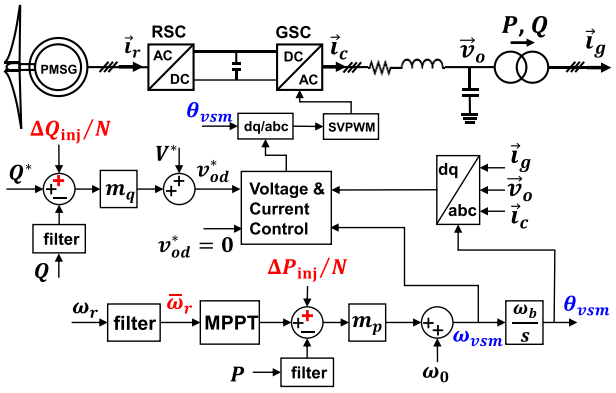

FIGURE 7. Control structure of the proposed Forced Oscillation isolation and suppression in a PMSG-based WTS under grid-forming control.

amplitude, and can function in the absence of synchronous generators.

P/f and Q/V droop controls, as an example grid-forming control, are used in the GSC in Fig. 7. Other grid-forming control, e.g. virtual oscillator control, dispatchable virtual oscillator control, synchronous machine emulation, etc. could also be used in the GSC. Without the discussed Forced Oscillation isolation and suppression method, to maximize wind power capture in a WTS, the traditional P/f and Q/V droop controls [29] are modified as

$$\omega_{vsm} = \omega_0 + m_p(K_{opt}\omega_r^3 - \frac{\omega_c}{s+\omega_c}P) \tag{29}$$

$$v_{od}^* = V^* + m_q(Q^* - \frac{1}{T_Q s+1}Q) \tag{30}$$

where ω_b, ω_0, and ω_{vsm} are the base and nominal angular frequency, and virtual angular speed, while m_p and m_q are the active and reactive droop gains. m_c and T_Q are the cut-off frequency and time constant of the low-pass filters, associated with filtering the active and reactive output power P and Q signals. $K_{opt}\omega_r^3$ in (29) is for implementing MPPT control.

With the discussed Forced Oscillation isolation and suppression method, the P/f and Q/V droop controls implemented in a WTS are given as

$$\omega_{vsm} = \omega_0 + m_p(K_{opt}\overline{\omega}_r^3 + \frac{\Delta P_{inj}}{N} - \frac{\omega_c}{s+\omega_c}P) \tag{31}$$

$$v_{od}^* = V^* + m_q(Q^* + \frac{\Delta Q_{inj}}{N} - \frac{1}{T_Q s+1}Q) \tag{32}$$

where N, ΔP_{inj}, ΔQ_{inj} and $\overline{\omega}_r$ are the same as that in (28)(29) for a grid-following control based WTS.

In (27)(28) and (31)(32), $1/N$ can be replaced by $\omega_i^2 S_{Hi}/\sum_{j=1}^{N}\omega_j^2 S_{Hj}$ to adaptively allocate the task of Forced Oscillation isolation and suppression to individual WTSs in a wind farm according to their stored kinetic energy and converter capacity headroom, where ω_i and ω_j are rotor speeds, and S_{Hi} and S_{Hj} are the available capacity headroom above the current operating point of the grid-side converter GSC of the i^{th} and j^{th} WTS.

In the GSC in Fig. 7, with the P/f and Q/V droop controls as outer control loop, the cascaded voltage and current controls are used for the inner control loops. Current limiting control for protecting the GSC from overloading is also added in the inner control loops. As in the outer control loop, other functions, e.g. system damping enhancement, secondary and third frequency regulation, voltage secondary regulation, etc. can also be added.

IV. CASE STUDIES

The modified two-area and IEEE 39-bus power systems, as shown in Fig. 8 and Fig. 9, respectively, are used to investigate the performance of the proposed method. The system parameters are the same as that in [30] and [31], where all the synchronous generators are equipped with a high transient gain thyristor exciter and a STAB1 PSS to ensure a good damping. The parameters of the DFIG- and PMSG-based WTSs are the same as those in [32], [33], which are provided in Table 1 in the Appendix.

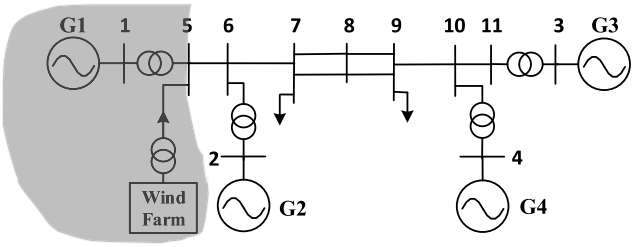

FIGURE 8. Structure of the two-area system with a DFIG-based WF located at bus 5.

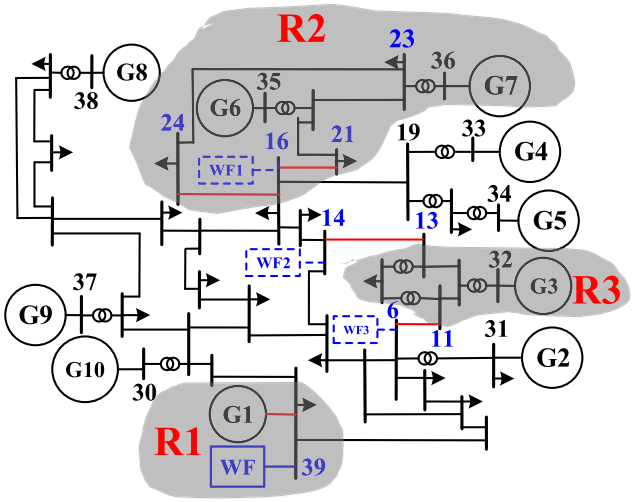

FIGURE 9. Structure of the modified IEEE 39-bus power system when a PMSG-based WF is located at bus 39 under Case 4 & 7, or at bus 16 under Case 5 & 6, or three WFs are located at bus 16, 14 and 6 under Case 8.

In the following, three case studies based on the two-area system are carried out in a real-time digital simulator (RTDS) platform, and four cases based on the 39-bus system are carried out in Dymola, to demonstrate the effectiveness of the proposed method. In the following simulation results,

Ti-j means transmission line between bus i and bus j and Pi,j means the transmitted power of Ti-j, the time x-axis is in the unit of seconds, and "@N" and "@Y" mean without and with the proposed method implemented, respectively.

A. SIMULATIONS BASED ON THE TWO-AREA SYSTEM WITH A DFIG-BASED WF

Case 1 - 3 are simulated based on the two-area system [30], which is modified by installing a DFIG-based WF at bus 5. The WF consists of 500 DFIG-based WTSs (i.e. 1000 MW) with an input wind speed of 10 m/s (between cut-in wind speed of 6 m/s and rated wind speed of 12 m/s). Moving average filters with time window of 20 s are used to obtain ΔP_{inj}, ΔQ_{inj} and the average rotor speed in (28), (29), (32) and (33).

1) ISOLATION AND SUPPRESSION OF FORCED OSCILLATIONS BY ONLY INJECTING ACTIVE POWER OF THE DFIG-BASED WF

Case 1: In this case, the WF is located at bus 5 in Fig. 8. An external sinusoidal disturbance $0.04\sin(0.67 * 2\pi t)$ pu (0.04 pu is equal to 36MW) is added to the mechanical torque of G1 from 65s to 95s to cause Forced Oscillations. In this case, only oscillating active power is injected from WF with $\Delta P_{inj} = -\Delta P_{15}$ under the proposed strategy. Therefore, transmission line T1-5 is the *isolation wall* in this case, through which the oscillations from G1 cannot be propagate to the rest of the system, and the oscillations from the rest of system cannot excite oscillations in G1.

The simulation results for Case 1 are shown in Fig. 10. Fig. 10(c) ∼ Fig. 10(f) show that without the proposed control scheme, both active and reactive power output of G1 ∼ G4 are excited by Forced Oscillations with big amplitudes, even when the system has good damping performance. The phenomenon verifies the conclusion from Fig. 3 and in [3] that the method of increasing damping to suppress Forces Oscillations is not effective. By contrast, Fig. 10(c) ∼ Fig. 10(f) show that with the proposed method, the oscillating active power of G2 ∼ G4 are reduced to zero and the oscillating reactive power are also reduced to nearly zero. This is because the WF generates oscillating active power ΔP_{WF} opposite to ΔP_{15}, as seen from Fig. 10(b), making ΔP_{56} zero (Fig. 10(a)). Thus, the active power components of Forced Oscillations are contained (isolated) before bus 5 (the grey area shown in Fig. 8) and are not spreading beyond bus 5. At the same time, Forced Oscillations before bus 5 are also suppressed, which can be seen from Fig. 10(c) and Fig. 10(e), where active power oscillations in P_{g1} and reactive power oscillations in Q_{g1} are only 0.6 times and 0.15 times of that without the proposed control respectively. Since $P_{15} = P_{g1}$, the suppression in P_{g1} means that the injected extra active power from the WF ΔP_{inj} only 0.6 times of that in P_{g1} without the proposed scheme. Fig. 10 shows the oscillations in the reactive power output of G2 ∼ G4 are greatly reduced when only active power of the WF is injected. This verifies that Forced Oscillations are mainly associated with active power.

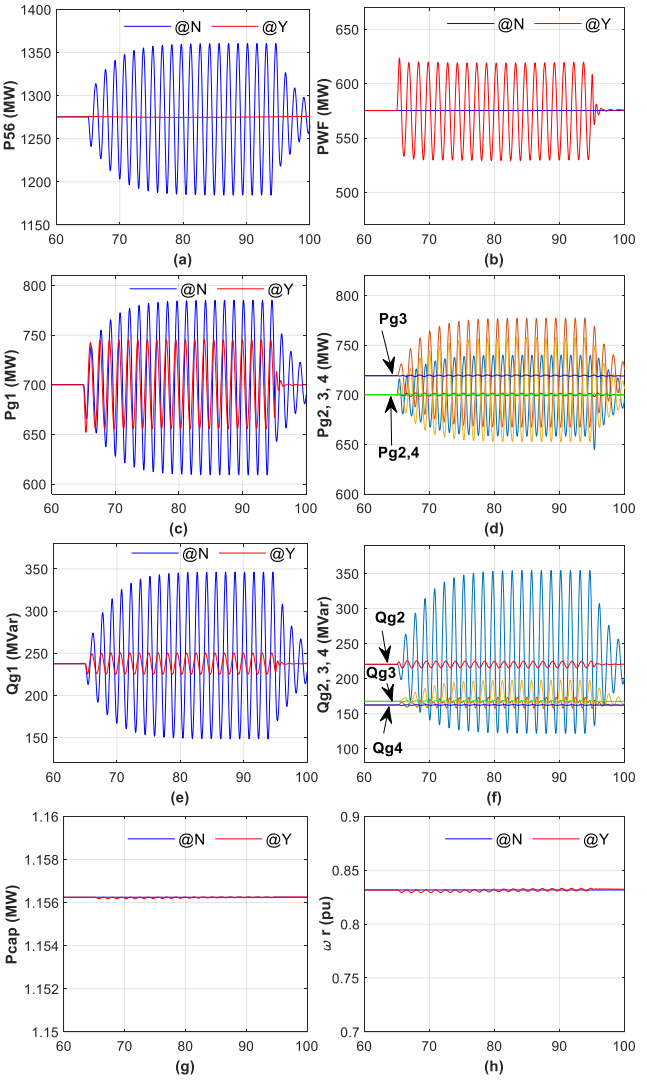

FIGURE 10. Simulation results without the proposed control ("N") and with active power injection of the WF ("Y") under Case 1.

Fig. 10(b) shows that the magnitude of ΔP_{WF} is around 40 MW, so each WTS injects extra oscillating power of 0.08 MW (40 / 500). Thus 3.2% extra capacity of the converters in a WTS is needed (3.2% = 0.08 MW / 2.5 MW since a WTS with a wind turbine of 2.0 MW rated capacity is usually equipped with converters of 2.5 MW rated capacity). This is practically feasible considering that the extra capacity is small, and the ongoing trend is that extra functions are required to be added into WTSs by grid codes, e.g. voltage and frequency regulation, which also unavoidably requires extra capacity of converters in WTSs. Fig. 10(g) and Fig. 10(h) show the loss of wind power capture and the change of rotor speed are very small. This verifies the performance of the proposed method.

2) WF BEING THE FORCED OSCILLATION SOURCE

Case 2: In this case, the DFIG-based WF is located at bus 5 in Fig. 8 and a sinusoidal disturbance $1.5\sin(0.6 * 2\pi t)$ m/s

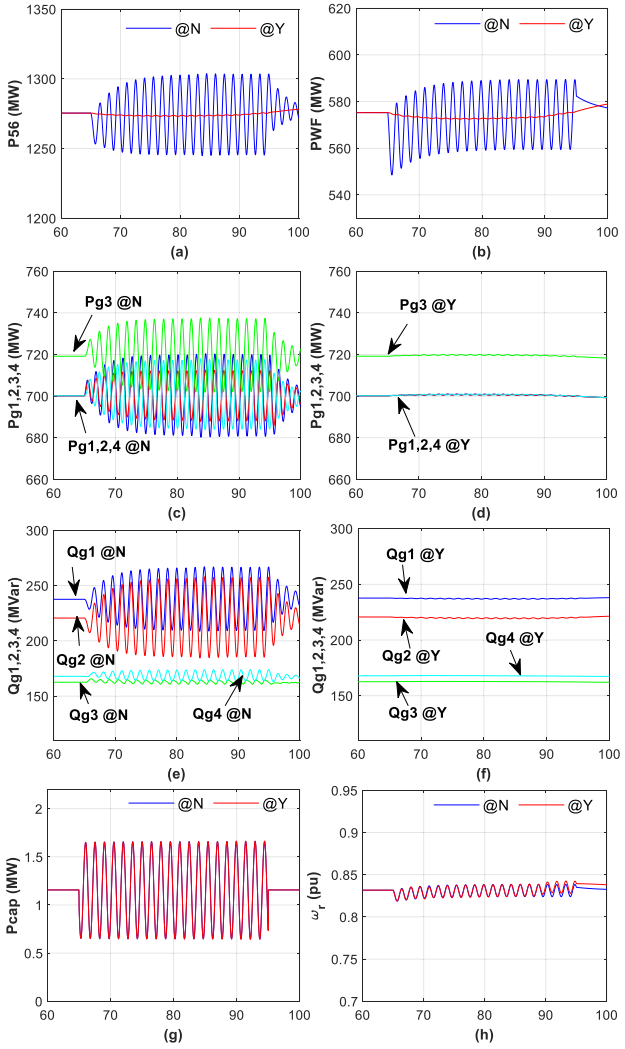

FIGURE 11. Simulation results under Case 2.

is added to the constant wind speed of 10 m/s from 65 s to 95 s. Thus, the WF becomes the Forced Oscillations source instead of G1. Under the proposed control, the oscillating power of WF can be smoothed before output to the grid and causing Forced Oscillations.

Fig. 11(a) $\sim$ Fig. 11(c) show that if the oscillating wind power from the WF is not smoothed, big Forced Oscillations are excited in P_{56}, $P_{g1} \sim P_{g4}$, and Q_{56}, $Q_{g1} \sim Q_{g4}$, while if the oscillating wind power is smoothed, no such oscillations are excited. The very small oscillations in wind power output under the proposed control (Fig. 11(b)) are due to the small oscillations in $\overline{\omega_r}$ caused by the imperfect filter.

Fig. 11(g) shows that the captured wind power under the proposed control is almost the same as that without the proposed control. Fig. 11(g) and Fig. 11(h) show that although the change of captured wind power is very big, the change of rotor speed in a WTS is small.

3) SUPPRESSION OF INTER-AREA OSCILLATIONS

Case 3: This case is simulated to verify that the proposed method can also help to damp inter-area oscillations. To excite inter-area oscillations, a 0.004 pu voltage step with a duration of 500 ms is added to the field voltage of G1. The DFIG-based WF is installed at bus 5 in Fig. 8 with both active and reactive power injection.

The simulation results of Case 3 are shown in Fig. 12. Fig. 12(a) and Fig. 12(b) show that by using the proposed Forced Oscillations isolation and suppression strategy, the inter-area oscillations are also well damped. Moreover, the WF has nearly zero loss of wind power capture, as demonstrated by Fig. 12(d). Comparing Fig. 12(c) with Fig. 12(a) and Fig. 12(b), it is seen that the duration of oscillations excited by G1 becomes shorter than that without the proposed scheme.

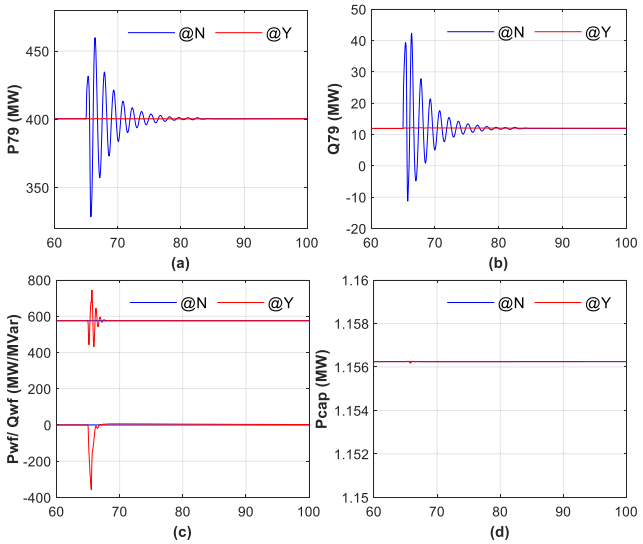

FIGURE 12. Simulation results under Case 3 with and without the proposed control.

B. SIMULATIONS BASED ON THE 39-BUS SYSTEM WITH PMSG-BASED WFS

Case 4 - 8 are simulated based on the 39-bus system [31]. Each WF used in this subsection consists of 500 PMSG-based WTSs. The variable wind speed input used in the following is taken from [34] (the cut-in and rated wind speed are 6 m/s and 12 m/s). In Case 4 - 8 under the proposed method, a 4th-order low-pass butterworth filter is used to obtain to ΔP_{inj}, and 2th-order low-pass butterworth filters are used to obtain ΔQ_{inj} and the average rotor speed of a WTS. For Case 4 -7, the cut-off frequency of those low-pass filters is 0.2 Hz, which is less than the minimum of the frequency spectrum of the Forced Oscillations considered in this paper. For Case 8, the cut-off frequency for the filters will be illustrated in that case.

1) ISOLATION AND SUPPRESSION OF FORCED OSCILLATIONS BY A GRID-FOLLOWING WF AT BUS 39

Case 4: In this case, the WF is located at bus 39. The used variable wind speed input is shown in Fig. 13(a). A sinusoidal disturbance $1.5\sin(1.4 * 2\pi t)$m/s is added to the variable

wind speed from 45 s to 80 s. Thus, during 45 $\sim$ 80 s the WF becomes a Forced Oscillations source. During 95 $\sim$ 130 s, an external sinusoidal disturbance $0.04\sin(1.4 * 2\pi t)$ pu (0.04 pu is equal to 40 MW) is added to the mechanical torque of G1 at Bus 39 to cause Forced Oscillations. In this case, the active and reactive power from G1 are chosen to be smoothed by the WF under the proposed method, i.e. ΔP_{G1} and ΔQ_{G1} are sent to the WF as ΔP_{inj} and ΔQ_{inj} in (1) and (2), respectively. Therefore, the line from bus 39 to G1 is the *isolation wall* in this case, beyond which the oscillations from G1 cannot be propagate to the other part of the system, and the oscillations from other part cannot excite oscillations in G1.

The simulation results for Case 4 are shown in Fig. 13. During 95 $\sim$ 130 s, Fig. 13(b)(c) show that without the proposed control method, both active and reactive power output of G10 at Bus 30 are oscillating with high amplitudes due to the Forces Oscillations from G1, even when the system has good damping, similar to that in Case 1. By contrast, Fig. 13(b)(c) show that with the proposed method, the oscillating active and reactive power of G10 are reduced to zero during 95 $\sim$ 130 s. This is because the WF generates oscillating active and reactive power opposite to the oscillating active and reactive power from the Forced Oscillations source of G1 at bus 39, as seen from Fig. 13(d) - (g). Thus, the Forced Oscillations caused by G1 are contained (isolated) before Bus 39 (the grey area indicated by R1 shown in Fig. 9) and are not spreading beyond bus 39. This can be seen from Fig. 13(h)(i) where the sum of the active and reactive power of T39-1 (which means transmission line between bus 39 and bus 1) and T39-9 is smoothed. At the same time, Forced Oscillations before bus 39 are also suppressed, which can be seen from Fig. 13(f)(g), where active and reactive power oscillations in the output active and reactive power of G1 at bus 39 are also reduced. Fig. 13(j) shows the rotor speed with the proposed method is close to that without the proposed method due to the fact that the stored kinetic energy of a WTS is much larger than the energy required to smooth the oscillating active power output of G1. This means that no extra mechanical pressure is added on a WTS under the proposed method and the loss of wind power is negligible as can be seen from Fig. 13(k). Fig. 9(l) shows that during 95 $\sim$ 130 s there are periods when the pitch angle control is effective. This illustrates that the proposed method is also effective under wind speeds higher than the rated one.

Fig. 13(d) and Fig. 13(e) show that during 95 $\sim$ 130 s the magnitude of the total oscillating power in Forced Oscillations frequency, i.e. $(\Delta P_{wf}^2 + \Delta Q_{wf}^2)^{0.5}$ is around 50 MVA, so each WTS injects extra oscillating power of 0.1

MVA (50 / 500). Thus 4% extra capacity of the converters in a WTS is needed (4% = 0.1 MVA / 2.5 MVA since a WTS has 2.5 MVA rated capacity). As explained in Case 1, this is practically feasible.

During 45 $\sim$ 80 s, Fig. 13(d) shows that without the proposed method the WF generates oscillating wind power and is the Forced Oscillations source. Thus, the active and reactive power of G1 and G10 are oscillating, as can be seen from Fig. 13(b)(c) and Fig. 13(f)(g). However, with the proposed method Fig. 13(d) shows that the WF outputs smoothed active

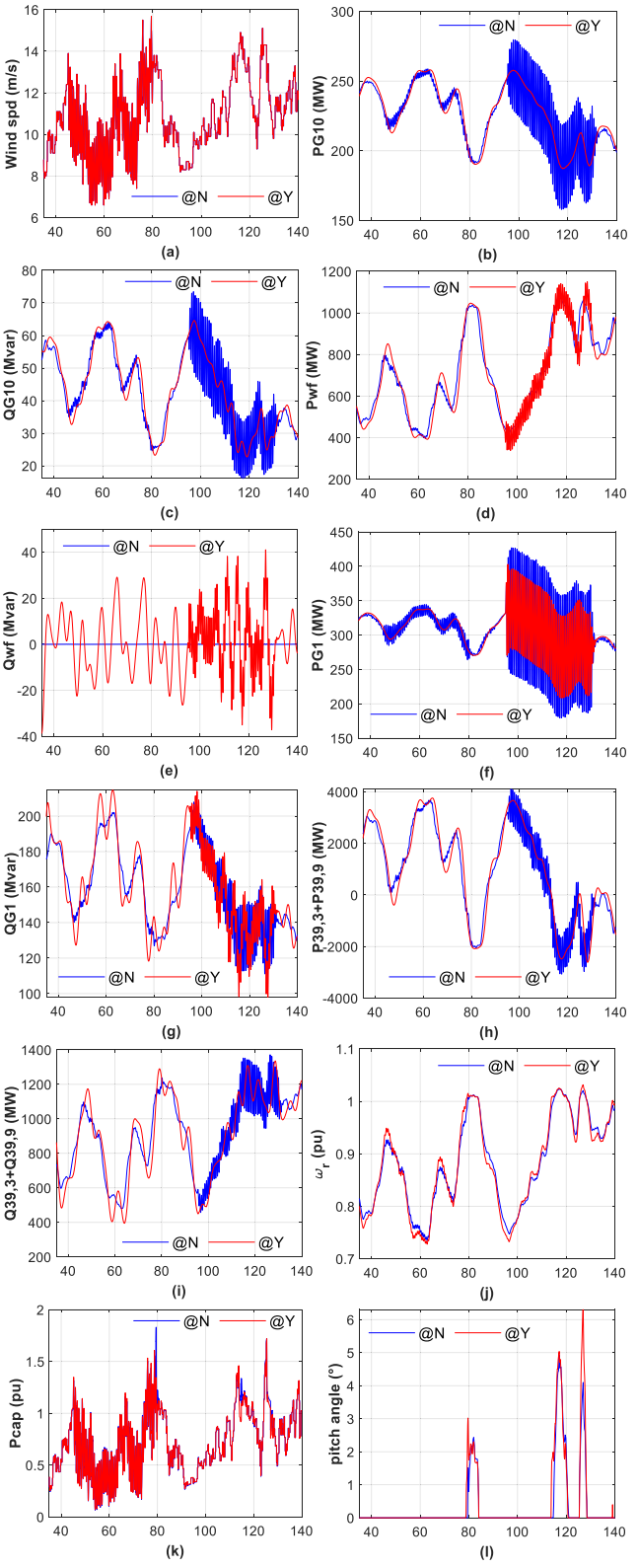

FIGURE 13. Simulation results without ("N") and with the proposed method ("Y") of WF under grid-following control for Case 4.

power by using the average instead of real-time rotor speed. Thus, the WF is no longer the Forced Oscillations source, which is demonstrated by the smoothed active and reactive power output of G1 and G10 shown in Fig. 13(b)(c) and Fig. 13(h)(i), respectively, and the smoothed active and reactive power of transmission lines of T39-1 and T39-9 shown in Fig. 13(f)(g).

Note that the active power of G10 changes considerably. This is because 1) the wind speed given for the wind farm is changing very large in a wide range from 8 m/s to 12.5 m/s (note that the cut-in wind speed is 6 m/s and rated wind speed is 12 m/s). Therefore, the power output of the wind farm changes very large considerably within 140 s window, as can be seen in Fig. 13(d); 2) the rated capacity of the wind farm is equal to that of G1-G10, which is 1000 MW.

2) ISOLATION AND SUPPRESSION OF FORCED OSCILLATIONS BY A GRID-FOLLOWING WF AT BUS 16

Case 5: In this case, an external sinusoidal disturbance $0.04\sin(1.4 * 2\pi t)$ pu is added to the mechanical torque of G7 during period of 60 $\sim$ 95 s to cause Forced Oscillations. The WF is located at bus 16, which is further away from the source of Forced Oscillations - G7. In this case, transmission lines of T16-24 and T16-21 are chosen to be the *isolation walls*, i.e. the sum of the oscillating active and reactive power at transmission lines of T16-24 and T16-21 are sent to the WF to generate oscillating power opposite to the sum to isolate the oscillating power beyond T16-24 and T16-21. Fig. 14(a) shows the used variable wind speed input.

The simulation results of Case 5 are shown in Fig. 14. It is seen that the proposed Forced Oscillations suppression and isolation performance is similar to that of Case 4, although the WF is far away from the oscillation source - G7. Fig. 14(b)(c) show that during 60 $\sim$ 95 s without the proposed method, G4 at bus 33 generate oscillating active and reactive power due to the Forced Oscillation from G7 at bus 36. On the contrary, under the proposed method, the active and reactive power of G4 are no longer oscillating. This is because under the proposed control method the WF at bus 16 generates oscillating power opposite to the oscillating power of transmission lines T16-24 and T16-21, as can be seen from Fig. 14(d)(e). In this way, the transmission lines of T16-24 and T16-19 become *isolation walls* through which Forced Oscillations excited by the external disturbance on G7 cannot propagate, as can be seen from Fig. 14(f)(g) that the active and reactive power of the transmission lines T16-17, T16-15 and T16-19 are smoothed under the proposed method. Thus, the Forced Oscillations excited by G7 are prevented from propagating beyond the *isolation walls* and isolated within the grey region i.e. R2 shown in Fig. 9. Fig. 14(h) shows the captured wind power with and without the proposed method are almost the same, indicating negligible loss of wind power capture.

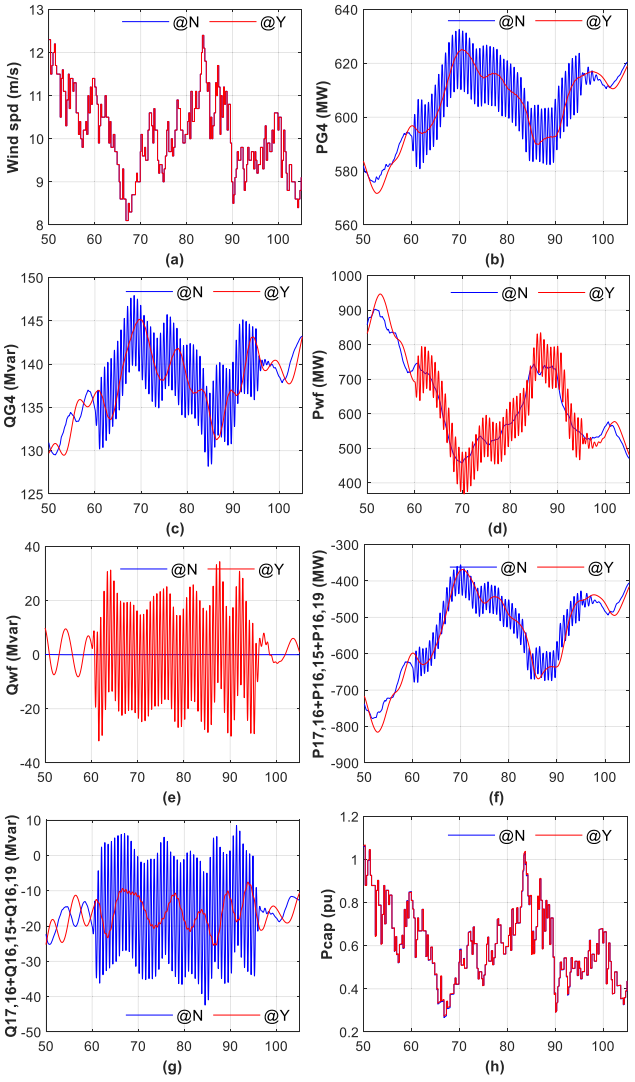

FIGURE 14. Simulation results without ("N") and with the proposed method ("Y") of WF under grid-following control, located at bus 16, under Case 5.

3) SUPPRESSION OF INTER-AREA OSCILLATIONS BY A GRID-FOLLOWING WF AT BUS 16

Case 6: This case is simulated to verify that the proposed method can also help to damp inter-area oscillations. To excite inter-area oscillations, a three-phase fault with a duration of 100 ms is triggered at bus 23. The WF is located at bus 16 with a constant wind speed of 10 m/s.

The simulation results of Case 6 are shown in Fig. 15. Fig. 15(a)(b) show that using the proposed Forced Oscillations isolation and suppression method, the inter-area oscillations are also well damped, similar to that in Case 3. This is because the WF smooths the active and reactive power of transmission lines of T16-24 and T16-21 by generating oscillating power opposite to that of the latter under the proposed control method as can be seen from Fig. 15(c)(d).

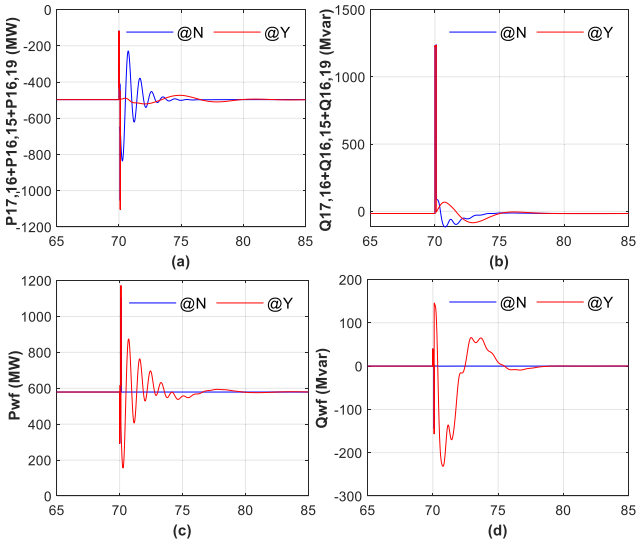

FIGURE 15. Simulation results for Case 6 with and without the proposed Forced Oscillation isolation and suppression method of WF under grid-following control.

4) ISOLATION AND SUPPRESSION OF FORCED OSCILLATIONS BY A GRID-FORMING WF AT BUS 39

Case 7: To demonstrate the effectiveness of the proposed Forced Oscillation isolation and suppression method by grid-forming control based WTSs, the 39-bus system in Fig. 9 is simulated, where a WF is located at bus 39 and consists of 500 PMSG-based WTSs under the droop-based grid-forming control shown in Fig. 7. During 30 $\sim$ 60 s, an external sinusoidal disturbance $0.04\sin(1.4*2\pi t)$ pu is added to the mechanical torque of G1 at bus 39 to cause Forced Oscillations. The active and reactive power from G1 are chosen to be smoothed by the WF under the disclosed method, i.e. $-\Delta P_{G1}$ and $-\Delta Q_{G1}$ are sent to the WF as ΔP_{inj} and ΔQ_{inj} in (1) and (2), respectively. Therefore, the line from bus 39 to G1 is the *isolation wall* in this case.

For the grid-forming control based WTS, the parameters of the GSC are: $m_p = 0.02$, $m_q = 0.0001$, $V_{ref} = 1\ pu$, $\omega_c = 31.4\ rad/s$, $T_Q = 1/31.4\ s$, $\omega_b = 314\ rad/s$, $\omega_0 = 1\ pu$, the proportional-integral gains for the inner voltage and current controllers are 0.52 pu, 1.16 pu, and 0.74 pu, 1.19 pu. The parameters of the LCL filter of the GSC are $R_f = R_c = 0.005\ pu$, $L_f = R_c = 0.15\ pu$ and $C_f = 0.066\ pu$.

Fig. 16(a) and (b) show the simulation comparison of the active and reactive power outputs of the synchronous generator G10 at bus 30 when the WF is under either the grid-forming or grid-following control, without and with the proposed Forced Oscillation isolation and suppression method. Without the proposed Forced Oscillation isolation and suppression method for the WF under the grid-forming control, Fig. 16 shows that the active and reactive power oscillations of G10 at bus 30 are already reduced. This shows the benefit of suppressing oscillations by just including grid-forming control based WTSs even without using the proposed Forced Oscillation isolation and suppression method in a power system.

Using the proposed isolation and suppression method for the WF, Fig. 16 shows the oscillations in active and reactive power outputs of G10 are greatly reduced no matter the WF is under grid-following or grid-forming control, while the oscillations are almost eliminated when the WF is under grid-following control. This is because grid-following control based WTS can inject oscillating power exactly opposite to that of the isolation walls, while grid-forming control based WTS cannot inject the exact opposite power because the grid frequency cannot be fixed at the normal frequency when power oscillations exist in the system, according to the grid-forming control principle in Fig. 7. This case has demonstrated that grid-forming control based WTSs using the proposed method can also isolate and suppress Forced Oscillations very well.

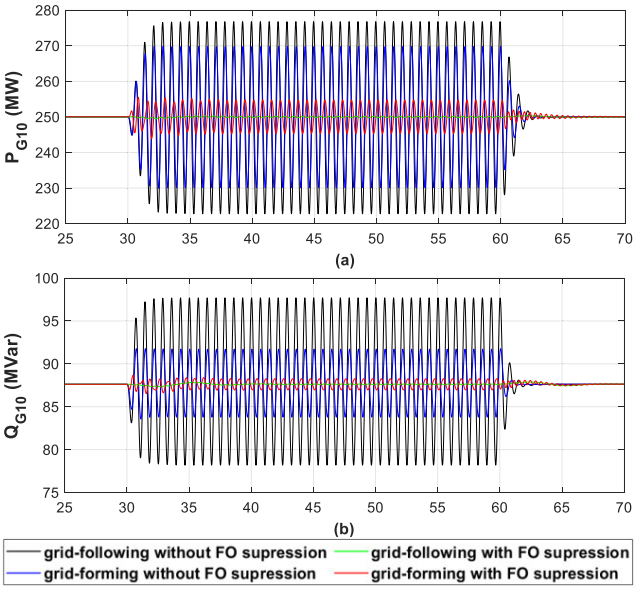

FIGURE 16. Simulation results for Case 7 with and without the proposed Forced Oscillation isolation and suppression method of WF under either the grid-forming or grid-following control.

5) ISOLATION AND SUPPRESSION OF MULTIPLE FORCED AND INTER-AREA OSCILLATIONS WITH VARYING FREQUENCIES AND AMPLITUDES

Case 8: In this case, external sinusoidal disturbances $0.04\sin(f_{G3}*2\pi t)$ pu, $0.02\sin(f_{G6}*2\pi t)$ pu and $A_{G7}\sin(f_{G7}*2\pi t)$ pu are added to the mechanical torque of G3, G6, and G7 in the 39-bus system, respectively, during the period of 60 $\sim$ 95 s to cause Forced Oscillations. f_{G3} is changed from 0.4 Hz to 1.0 Hz at 80 s, f_{G6} from 1.1 Hz to 0.7 Hz at 75 s, f_{G7} from 1.4 Hz to 1.2 Hz, and A_{G7} from 0.02 pu to 0.04 pu. WF1, WF2 and WF3 are located at buses 6, 14, and 16, respectively. WF1 at bus 16 is chosen to isolate the Forced Oscillations from G6 and G7, by smoothing the oscillating active and reactive power at transmission lines of T16-24 and T16-21. WF2 and WF3 at buses 6 and 14 are chosen to

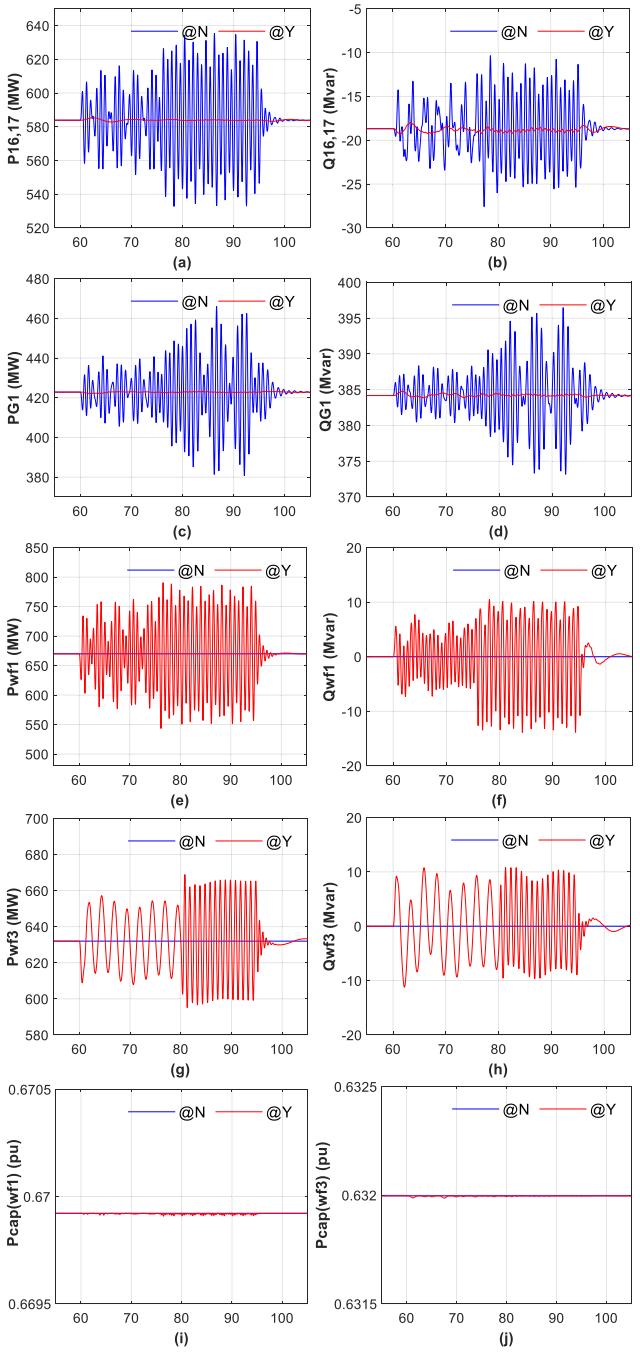

FIGURE 17. Simulation results for Case 8 with and without the proposed Forced Oscillation isolation and suppression method of WF under either the grid-forming or grid-following control.

isolate the Forced Oscillations from G3, by smoothing the oscillating active and reactive power at transmission lines of T6-11 and T14-13, respectively. Therefore, T16-24, T16-21, T6-11 and T14-13 are the *isolation walls*, beyond which the Forced Oscillations are isolated in the shadow areas R2 and R3 shown in Fig. 9 under the proposed method. Based on the frequencies of the disturbances in this case, the cut-off frequency of the low-pass filters to obtain ΔP_{inj}, ΔQ_{inj} and the average rotor speed in (28), (29), (32) and (33) for WF1 at bus 16 is still 0.2 Hz, but for WF2 and WF3 is 0.1 Hz.

The simulation results of Case 8 are shown in Fig. 17. In order to show the Forced Oscillations isolated within the grey areas R2 and R3, the active and reactive power of the transmission line T16-17 and G1 are chosen to be shown in Fig. 17(a)(b) and Fig. 17(c)(d). It is seen that under the proposed Forced Oscillation isolation and suppression method they are well smoothed. This demonstrates that the proposed method can isolate and suppress multiple Forced Oscillations with different and varying frequencies and amplitudes without the detection of the oscillations. Fig. 17(e)(f) and Fig. 17(g)(h) show that under the proposed method, WF1 and WF3 generate oscillating active and reactive power opposite to that of the sum of the transmission lines T16-24 and T16-21, and that of the transmission line T6-11, respectively. The power output of WF2 is similar to that of WF3 and thus not shown. Fig. 17(i)(j) show that the captured power of WF1 and WF3 with the proposed method are nearly the same as that without the proposed method, demonstrating the negligible loss of wind power capture. Note that since inter-area oscillations are in the range of 0.2 – 0.8 Hz, which is emulated by f_{G3} and f_{G6}, this case demonstrates that the proposed method can isolate and suppress Forced and inter-area oscillations simultaneously.

V. CONCLUSION

With increasing high penetration of renewable energy generation towards 100% renewable generation in the power grid, exploitation of future control potential from wind turbines becomes inevitable. The key contributions of the proposed method are:

- This paper has proposed an isolation and suppression method for Forced Oscillations using WFs;
- By controlling WFs to release or absorb active and reactive power opposite to the oscillating power from the selected *isolation wall*, the Forced Oscillations are isolated within the disturbed area and hence are prevented from propagating to the rest of the system. Meanwhile, the Forced Oscillations excited in the disturbed area (which is bounded by the location of WF installation) are also reduced and suppressed;
- The proposed method can be implemented in WTSs under either grid-following or grid-forming control principle;
- The effectiveness of the proposed method was supported and explained by theoretical analysis first. Then the modified two-area power system with a DFIG-based WF and the IEEE 39-bus power system with PMSG-based WFs under either grid-following or grid-forming control principle was simulated using RTDS and Dymola. The simulation results considering variable wind speed input, different WF locations with respect to the source of Forced Oscillations, and multiple Forced Oscillations with varying frequencies and amplitudes, demonstrated that the proposed method can isolate and suppress Forced Oscillations and damp inter-area oscillations

very well, while the loss of wind power capture is negligible and only a small increase of the converter capacity by 4% is needed, which should be within the normal design rating of the converter;

- The isolation and suppression method is also applicable to other controllable devices. For example, it can be directly implemented in grid-interfacing converter systems such as energy storage systems, PV generation systems, HVDC, FACTS, etc.

APPENDIX

TABLE 1. Parameters of DFIG- and PMSG-based WTSs.

DFIG-base WTS	Value	PMSG-base WTS	Value
Rated capacity of the turbine/DFIG	2.0 MVA/ 2.2 MVA	Rated capacity	2.0 MVA
Rated stator voltage	0.69 kV	Rated stator voltage	4 kV
Rated frequency	50 Hz	Rated frequency	3.77 Hz
Stator/rotor resistance	0.00462 pu/ 0.006 pu	Pole pair	11
Stator/rotor leakage inductance	0.102 pu/ 0.08596 pu	Stator resistance	0.01 pu
Mutual inductance	4.348 pu	Stator leakage inductance	0.1 pu
Wind turbine/DFIG inertia constant	4.3 s/0.75 s	D-/Q-axis unsaturated magnet. Inductance	0.65 pu /1.0 pu
		Magnetic strength	1.3 pu
		PMSG inertia constant	5.05 s

Captured wind power $P_{cap}=0.5\rho\pi R^2 v_w^3 C_\rho(\lambda,\beta) = Kv_w^3 C_\rho(v_w,\omega_r,\beta)$, where $K=0.0012$, v_w is in m/s, ω_r is in pu (when $v_w \geq 12m/s$, $\omega_r = 1pu$), $R=81m$, and $C_\rho \sim \lambda$ curve is adopted from [27].

REFERENCES

[1] P. Kundur, *Power System Stability and Control*. New York, NY, USA: McGraw-Hill, 1994.

[2] C. Vournas, N. Krassas, and B. C. Papadias, "Analysis of forced oscillations in a multimachine power system," in *Proc. Int. Conf. Control*, Edinburgh, U.K., vol. 1, Mar. 1991, pp. 443–448.

[3] S. Feng, X. Wu, P. Jiang, L. Xie, and J. Lei, "Mitigation of power system forced oscillations: An E-STATCOM approach," *IEEE Access*, vol. 6, pp. 31599–31608, 2018.

[4] H. Ye, Y. Liu, P. Zhang, and Z. Du, "Analysis and detection of forced oscillation in power system," *IEEE Trans. Power Syst.*, vol. 32, no. 2, pp. 1149–1160, Jun. 2017.

[5] M. A. Magdy and F. Coowar, "Frequency domain analysis of power system forced oscillations," *IEE Proc. C Gener., Transmiss. Distrib.*, vol. 137, no. 4, pp. 261–268, Jul. 1990.

[6] M. Ghorbaniparvar, "Survey on forced oscillations in power system," *J. Modern Power Syst. Clean Energy*, vol. 5, no. 5, pp. 671–682, Sep. 2017.

[7] D. S. L. Dolan and P. W. Lehn, "Simulation model of wind turbine 3p torque oscillations due to wind shear and tower shadow," *IEEE Trans. Energy Convers.*, vol. 21, no. 3, pp. 717–724, Sep. 2006.

[8] S. A. N. Sarmadi, V. Venkatasubramanian, and A. Salazar, "Analysis of November 29, 2005 western American oscillation event," *IEEE Trans. Power Syst.*, vol. 31, no. 6, pp. 5210–5211, Nov. 2016.

[9] S. A. N. Sarmadi and V. Venkatasubramanian, "Inter-area resonance in power systems from forced oscillations," *IEEE Trans. Power Syst.*, vol. 31, no. 1, pp. 378–386, Jan. 2016.

[10] X. Wang and K. Turitsyn, "Data-driven diagnostics of mechanism and source of sustained oscillations," *IEEE Trans. Power Syst.*, vol. 31, no. 5, pp. 4036–4046, Sep. 2016.

[11] T. R. Nudell, S. Nabavi, and A. Chakrabortty, "A real-time attack localization algorithm for large power system networks using graph-theoretic techniques," *IEEE Trans. Smart Grid*, vol. 6, no. 5, pp. 2551–2559, Sep. 2015.

[12] M. Ghorbaniparvar, N. Zhou, X. Li, D. J. Trudnowski, and R. Xie, "A forecasting-residual spectrum analysis method for distinguishing forced and natural oscillations," *IEEE Trans. Smart Grid*, vol. 10, no. 1, pp. 493–502, Jan. 2019.

[13] L. Chen, Y. Min, and W. Hu, "An energy-based method for location of power system oscillation source," *IEEE Trans. Power Syst.*, vol. 28, no. 2, pp. 828–836, May 2013.

[14] S. Roy, W. Ju, N. Nayak, and B. Lesieutre, "Localizing power-grid forced oscillations based on harmonic analysis of synchrophasor data," in *Proc. 55th Annu. Conf. Inf. Sci. Syst. (CISS)*, Mar. 2021, pp. 1–5.

[15] F. M. Hughes, O. Anaya-Lara, G. Ramtharan, N. Jenkins, and G. Strbac, "Influence of tower shadow and wind turbulence on the performance of power system stabilizers for DFIG-based wind farms," *IEEE Trans. Energy Convers.*, vol. 23, no. 2, pp. 519–528, Jun. 2008.

[16] T. Surinkaew, R. Shah, M. Nadarajah, and S. M. Muyeen, "Forced oscillation damping controller for an interconnected power system," *IET Gener., Transmiss. Distrib.*, vol. 14, no. 2, pp. 339–347, Jan. 2020.

[17] T. Surinkaew, R. Shah, S. M. Muyeen, N. Mithulananthan, K. Emami, and I. Ngamroo, "Novel control design for simultaneous damping of inter-area and forced oscillation," *IEEE Trans. Power Syst.*, vol. 36, no. 1, pp. 451–463, Jan. 2021.

[18] P. Jiang, Z. Fan, S. Feng, X. Wu, H. Cai, and Z. Xie, "Mitigation of power system forced oscillations based on unified power flow controller," *J. Modern Power Syst. Clean Energy*, vol. 7, no. 1, pp. 99–112, Jan. 2019.

[19] L. Zhu, W. Yu, Z. Jiang, C. Zhang, Y. Zhao, J. Dong, W. Wang, Y. Liu, E. Farantatos, D. Ramasubramanian, A. Arana, and R. Quint, "A comprehensive method to mitigate forced oscillations in large interconnected power grids," *IEEE Access*, vol. 9, pp. 22503–22515, 2021.

[20] J. Tan, X. Wang, T. Wang, and Y. Zhang, "Alleviation of oscillations power of wind farm using flywheel energy storage," in *Proc. IEEE PES Gen. Meeting Conf. Expo.*, Jul. 2014, pp. 1–5.

[21] C. Su, W. Hu, Z. Chen, and Y. Hu, "Mitigation of power system oscillation caused by wind power fluctuation," *IET Renew. Power Gener.*, vol. 7, no. 6, pp. 639–651, Nov. 2013.

[22] D. J. Trudnowski and R. Guttromson, "A strategy for forced oscillation suppression," *IEEE Trans. Power Syst.*, vol. 35, no. 6, pp. 4699–4708, Nov. 2020.

[23] J. A. Carta, P. Ramírez, and S. Velázquez, "A review of wind speed probability distributions used in wind energy analysis," *Renew. Sustain. Energy Rev.*, vol. 13, no. 5, pp. 933–955, Jun. 2009.

[24] E. C. Morgan, M. Lackner, R. M. Vogel, and L. G. Baise, "Probability distributions for offshore wind speeds," *Energy Convers. Manage.*, vol. 52, no. 1, pp. 15–26, Jan. 2011.

[25] M. Beza and M. Bongiorno, "An adaptive power oscillation damping controller by STATCOM with energy storage," *IEEE Trans. Power Syst.*, vol. 30, no. 1, pp. 484–493, Jan. 2015.

[26] N. P. W. Strachan and D. Jovcic, "Stability of a variable-speed permanent magnet wind generator with weak AC grids," *IEEE Trans. Power Del.*, vol. 25, no. 4, pp. 2779–2788, Oct. 2010.

[27] G. L. Johnson, *Wind Energy Systems*. Englewood Cliffs, NJ, USA: Prentice-Hall, 1985.

[28] R. Pena, J. C. Clare, and G. M. Asher, "Doubly fed induction generator using back-to-back PWM converters and its application to variable-speed wind-energy generation," in *Proc. IEE Proc., Elect. Power Appl.*, vol. 143, no. 3, pp. 231–241, May 1996.

[29] X. Zhao and D. Flynn, "Freezing grid-forming converter virtual angular speed to enhance transient stability under current reference limiting," in *Proc. IEEE 21st Workshop Control Modeling Power Electron. (COMPEL)*, Nov. 2020, pp. 1–7.

[30] P. Kundur, *Power System Stability and Control*. New York, NY, USA: McGraw-Hill, 1994.

[31] I. Hiskens. (Nov. 2013). *IEEE PES Task Force on Benchmark Systems for Stability Controls*. 39-Bus System New England Reduced Model. [Online]. Available: http://www.sel.eesc.usp.br/ieee/

[32] X. Zhao, Z. Yan, and X.-P. Zhang, "A wind-wave farm system with self-energy storage and smoothed power output," *IEEE Access*, vol. 4, pp. 8634–8642, 2016.

[33] X. Zhao, Y. Xue, and X.-P. Zhang, "Fast frequency support from wind turbine systems by arresting frequency nadir close to settling frequency," *IEEE Open Access J. Power Energy*, vol. 7, pp. 191–202, 2020.

[34] *An Aeroelastic Computer-Aided Engineering Tool for Horizontal Axis Wind Turbines*. Accessed: Mar. 19, 2015. [Online]. Available: https://nwtc.nrel.gov/FAST

XIANXIAN ZHAO received the B.Eng. degree from Central South University, China, in 2012, and the Ph.D. degree from the University of Birmingham, U.K., in 2018.

She is currently a Senior Power System Researcher with University College Dublin, Ireland. Her research interests include power systems modeling and stability analysis.

YING XUE (Member, IEEE) received the B.Eng. and Ph.D. degrees in electronic, electrical, and computer engineering from the University of Birmingham, in 2012 and 2016, respectively.

He is currently a Lecturer with the University of Birmingham. His main research interest includes HVDC modeling and control.

XIAO-PING ZHANG (Fellow, IEEE) is currently a Professor of electrical power systems with the University of Birmingham, U.K., the Director of smart grid with the Birmingham Energy Institute, and the Co-Director of the Birmingham Center for Energy Storage. He has coauthored the first and second editions of the monograph *Flexible AC Transmission Systems: Modeling and Control* (Springer, 2006 and 2012) and the book *Restructured Electric Power Systems: Analysis of Electricity Markets with Equilibrium Models* (IEEE Press/Wiley, 2010). His research interests include modeling and control of HVDC, FACTS, and wind/wave generation, distributed energy systems and market operations, and power system planning. He has been made a fellow of IEEE for contributions to modeling and control of high-voltage DC and AC transmission systems. He is also a fellow of IET. He has been an Advisor of the IEEE PES UK and Ireland Chapter and chairing the IEEE PES WG on Test Systems for Economic Analysis. He has been the Vice Chair of the IEEE PES Marine Transmission and Distribution Subcommittee. Recently, he has been appointed to the Expert Advisory Group of the U.K. Government's Offshore Transmission Network Review. He is also an IEEE PES Distinguished Lecturer on HVDC, FACTS, and wave energy generation.